Nanoscale

PAPER

View Article Online
View Journal

Cite this: DOI: 10.1039/c4nr06331g

Thickness-dependent mobility in two-dimensional MoS_2 transistors†

Dominik Lembke, Adrien Allain and Andras Kis*

Received 27th October 2014,
Accepted 2nd March 2015

DOI: 10.1039/c4nr06331g

www.rsc.org/nanoscale

Two-dimensional (2D) semiconductors such as mono and few-layer molybdenum disulphide (MoS_2) are very promising for integration in future electronics as they represent the ultimate miniaturization limit in the vertical direction. While monolayer MoS_2 attracted considerable attention due to its broken inversion symmetry, spin/valley coupling and the presence of a direct band gap, few-layer MoS_2 remains a viable option for technological application where its higher mobility and lower contact resistance are believed to offer an advantage. However, it remains unclear whether multilayers are intrinsically superior or if they are less affected by environmental effects. Here, we report the first systematic comparison of the field-effect mobilities in mono-, bi- and trilayer MoS_2 transistors after thorough *in situ* annealing in vacuum. We show that the mobility of field-effect transistors (FETs) based on monolayer MoS_2 is significantly higher than that of FETs based on two or three layers. We demonstrate that it is important to remove the influence of gaseous adsorbates and water before comparing mobilities, as monolayers exhibit the highest sensitivity to ambient air exposure. In addition, we study the influence of the substrate roughness and show that this parameter does not affect FET mobilities.

Introduction

Two-dimensional (2D) layers from the group of semiconducting transition metal dichalcogenides (TMDCs) are very promising building blocks for future nanoelectronics.[1,2] In contrast to graphene,[3] semiconducting TMDCs exhibit bandgaps in the 1–2 eV range, enabling devices with large I_{on}/I_{off} ratios.[1] Due to their atomic thickness, 2D materials allow superior electrostatic control and as such, 2D TMDCs represent the ultimate limit for transistor scaling.[4] To date, the most widely studied TMDCs has been MoS_2. Monolayer MoS_2 is a true 2D semiconductor only 6.5 Å thick, exhibiting a direct band gap of 1.8 eV.[5] Recently, FETs,[1] signal amplifiers[6] as well as logic circuits operating at room temperature based on mono-[7] and bilayers[8] of MoS_2 have been demonstrated. FETs operating in the technologically relevant gigahertz-range of frequencies and showing current, voltage and power amplification have been demonstrated as well.[9] MoS_2 exhibits current saturation[10] and a breakdown current density at least 50 times higher than copper.[10] Besides its very promising electronic and optoelectronic[11] properties, MoS_2 exhibits mechanical stiffness comparable to steel and a breaking strength close to the theoretical limit of solid state materials,[12] making MoS_2 and 2D TMDCs interesting for applications in flexible, transparent electronics. Even though there has been a soaring interest in its electronic properties, the dependence of the charge carrier mobility in MoS_2 on the number of layers remains unclear. While some reports claimed an increasing mobility with increasing number of MoS_2 layers,[8,13–15] the mobility values for monolayer devices in these reports (~10–20 $cm^2\ V^{-1}\ s^{-1}$) were significantly lower than values of ~60 $cm^2\ V^{-1}\ s^{-1}$ measured after *in situ* annealing in vacuum.[16]

Here, we compare the mobility in mono-, bi- and trilayer FETs that underwent thorough *in situ* annealing. *In situ* annealing has proven to be a very efficient way to improve the mobility, especially in monolayer devices.[16–18] By removing atmospheric contaminations, which significantly reduce the conductivity and mobility,[16,18,19] we can study the influence of other parameters such as the number of layers and substrate roughness.[20]

Experimentation

Mono-, bi- and trilayer MoS_2 were prepared by mechanical exfoliation of commercially available crystals of MoS_2. The flakes were deposited on a degenerately doped silicon substrate covered with 270 nm SiO_2. The SiO_2 substrate of ~50%

Electrical Engineering Institute, École Polytechnique Fédérale de Lausanne (EPFL), CH-1015 Lausanne, Switzerland. E-mail: andras.kis@epfl.ch

†Electronic supplementary information (ESI) available. See DOI: 10.1039/c4nr06331g

of the devices underwent chemical-mechanical planarization (Alpsitec E460) to establish an ultra-flat substrate (see Fig. SI 3 of ESI†). The MoS_2 layer thicknesses were determined by optical contrast referred to the SiO_2 substrate. The correlation between layer number and optical contrast has been determined previously by means of atomic force microscopy.[21] Au contacts with a thickness of 90 nm were fabricated using electron-beam lithography. After lift-off in acetone, samples were annealed in Ar atmosphere at 200 °C for 2 hours to improve the contact of the MoS_2/Au interface. Four-terminal devices were shaped applying 15 seconds of oxygen plasma after an additional electron-beam lithography step. Electrical characterization was carried out utilizing a NI PXI-4461 DAQ card in a home-built vacuum and *in situ* annealing chamber.

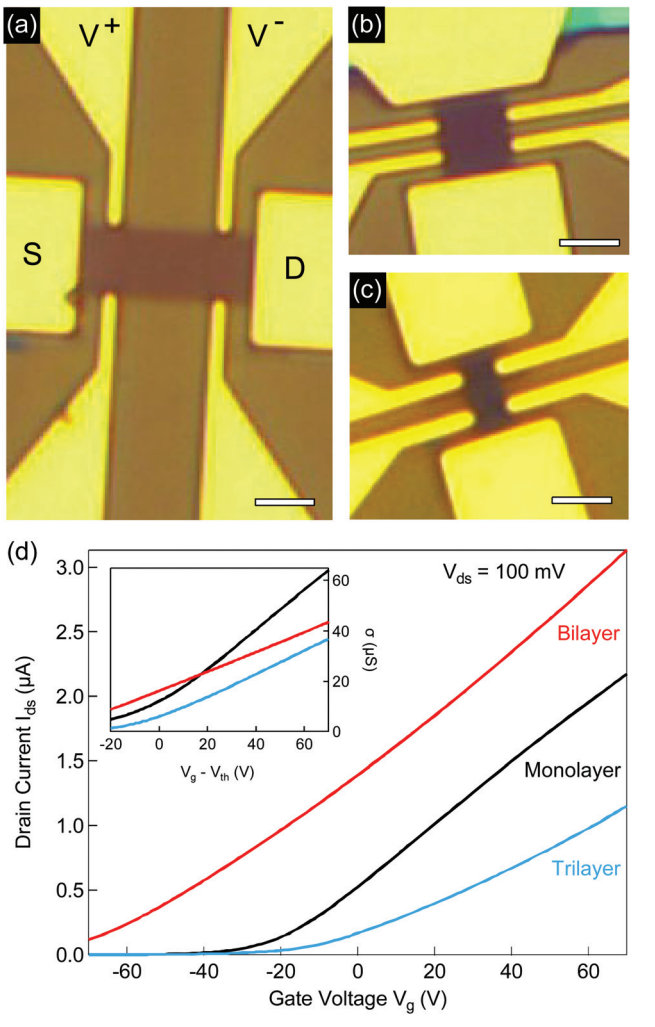

Fig. 1 Field-effect transistors (FETs) based on MoS_2. (a) Optical images of a monolayer, (b) bilayer and (c) trilayer (scale bars 2 μm) MoS_2 FET with Hall bar geometry. (d) Typical transfer-characteristics I_{ds} *vs.* V_g after annealing in vacuum (as discussed in the text) for FETs based on mono-, bi-, and trilayer MoS_2 at V_{ds} = 100 mV. Inset: Four-probe-conductivity σ *vs.* V_g for the same devices, as a function of gate overdrive voltage $V_g - V_{th}$.

Results and discussion

Fig. 1a–c depicts optical micrographs of typical multiterminal devices prepared for this study. It is important to note that this is the first study of thickness-dependent mobility in a four-terminal configuration. This allows extracting more accurate values of conductivity and mobility compared to two-terminal devices because the effect of contact resistance can be excluded.[22–24] Typical transfer characteristics (I_{ds} *vs.* V_g) are shown in Fig. 1d. The four-contact conductivity σ of the MoS_2 flakes can be deduced from $\sigma = \frac{L_{xx}}{W}\frac{I_{ds}}{V^+ - V^-}$, where L_{xx} is the spacing between the voltage probes, W the width of the channel, I_{ds} the drain–source current and V^+–V^- the potential drop between the two voltage probes. The inset of Fig. 1d displays the corresponding conductivities σ. From this, we can calculate the field-effect mobility as $\mu = \frac{1}{C_{ox}}\frac{d\sigma}{dV_g}$, where C_{ox} is the oxide capacitance. In the following discussion, we assume the geometric capacitance value to be $C_{ox} = \frac{\varepsilon_r \varepsilon_0}{d} = 1.3 \times 10^{-4}\,\mathrm{F\,m^{-2}}$, using ε_r = 3.9 and d = 270 nm for the dielectric constant and thickness of the SiO_2 layer.

Fig. 2 shows the influence of *in situ* annealing treatments on the performance of a monolayer FET. The red curve in Fig. 2a shows the four-contact conductivity σ under ambient conditions. Prior to characterization the device has been exposed to air for several days. We load the device in the vacuum chamber and pump to a vacuum level of $\sim 1 \times 10^{-5}$ mbar. Under these conditions, we expect most of the physisorbed gaseous molecules to be removed from the surface of the MoS_2. Removing the adsorbates results in a significantly improved conductivity (Fig. 2a) and mobility (Fig. 2c). Note that the above definition of the field-effect mobility μ is fully accurate only in the "on" state of the device. At this point, the measured characteristic is still hysteretic, giving rise to a mobility depending on the V_g sweep direction. Furthermore, the measurement is relatively noisy. Subsequently, the device is annealed at 120 °C for ~12 hours in vacuum and measured at a vacuum level of $\sim 1 \times 10^{-6}$ mbar after cool-down to room temperature. This annealing results in a shift of threshold-voltage V_{th}, corresponding to n-type doping.[18] The annealing eliminated the hysteric behavior of the device and the mobility is now independent of the V_g sweep direction. Now, we can also observe a plateau around the maximum value of field-effect mobility. This regime of carrier density-independent mobility is attributed to the conduction band mobility.[16] An extension of the annealing time does not result in a higher band mobility but in an even larger shift of V_{th}. We thus conclude that the extracted mobility value can be considered as the intrinsic mobility value of the characterized FET. This demonstrates the importance of thorough cleaning of 2D MoS_2 devices before comparing the performance of different device architectures. We rule out that the observed improvement of performance is due to improved contacts since we performed contact annealing prior to characterization. Fig. 2b and d show the conductivity and mobility after re-exposing the

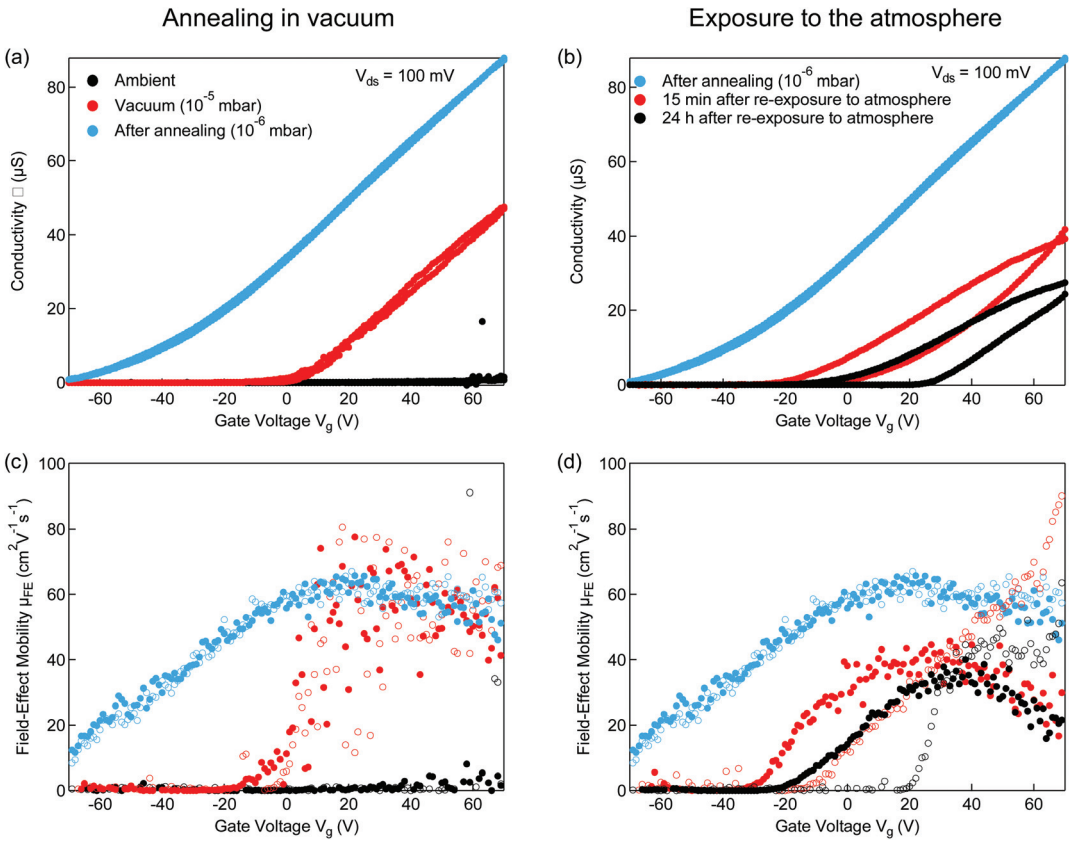

Fig. 2 Conductivity and mobility in a monolayer MoS_2 FET for each step during the process of cleaning and exposure to ambient. (a) Conductivity at different stages of vacuum annealing: right after fabrication (black curve), in vacuum before (red) and after (blue) overnight (~12 h) annealing at 120 °C. (b) Evolution of conductivity upon re-exposure to ambient: right after the cleaning process in vacuum (blue), after 15 min in air (red), after 24 h in air (black). (c) and (d) show corresponding field-effect mobilities. In (c) and (d), filled symbols represents the sweep from negative to positive back-gate voltage V_g, empty symbols correspond to the opposite sweep direction.

device to atmosphere for 15 minutes and 24 hours. This results in a significant reduction of conductivity and a shift of V_{th} towards positive voltages, indicating p-type doping. For longer exposures (~24 hours), the conductivity and mobility exhibit a gradual deterioration. For exposures exceeding 24 hours, we expect the device to eventually revert back to the original state, *i.e.* the situation prior to any vacuum cleaning and annealing. We made identical observations for all characterized devices investigated in this study (see section 2 and 3 of ESI†). The reversible change upon annealing/re-exposing to ambient conditions indicates that the threshold voltage change and hysteresis are due to adsorption/desorption of atmospheric species and not to the formation of atomic defects.

We observe the mobility plateau after *in situ* annealing (Fig. 3a) in all devices (see Fig. SI 2 of ESI†) and can use it as a reference point for comparison of the band mobility. Fig. 3b shows the band mobility values, averaged over a range of ΔV_g = 10 V around the maximum extracted mobility. The error bars correspond to the Gaussian error deduced assuming that the oxide thickness d_{ox}, the voltage probe spacing L_{xx} and the width W vary by ±20 nm, ±150 nm and ±150 nm, respectively. These parameters were checked by means of optical reflectometry (d_{ox}) and atomic force microscopy (L_{xx} and W), showing that these error assumptions are conservative estimates. The error bars specify the confidence interval of the mobility extraction but do not account for the scattering of the data points, which is caused by the influence of environmental factors. Fig. 3b shows that the band mobility in monolayer devices is significantly higher than in devices based on two and three layer thick MoS_2. We conduct a statistical *t*-test of this hypothesis and conclude that it is correct with a probability of 99.5% (see section 4 of ESI†). The observation of highest mobility in monolayer of MoS_2 is in contradiction with previous reports.[8,13,15,25,26] Among those reports, several[13,25,26] studied the thickness-dependent mobility systematically. All of them reported the opposite mobility trend for thin layers, *i.e.* a decreasing mobility with decreasing number of layers and a minimum for monolayers. As in all these previous studies the mobility of the monolayer remains well below the value reported here, we attribute this erroneous observations to insufficient removal of atmospheric adsorbates. We expect scattering caused by extrinsic charged impurities to decrease as the layer thickness increases. This assumption is supported by the fact that for much thicker layers (~10 nm)[13,25] higher

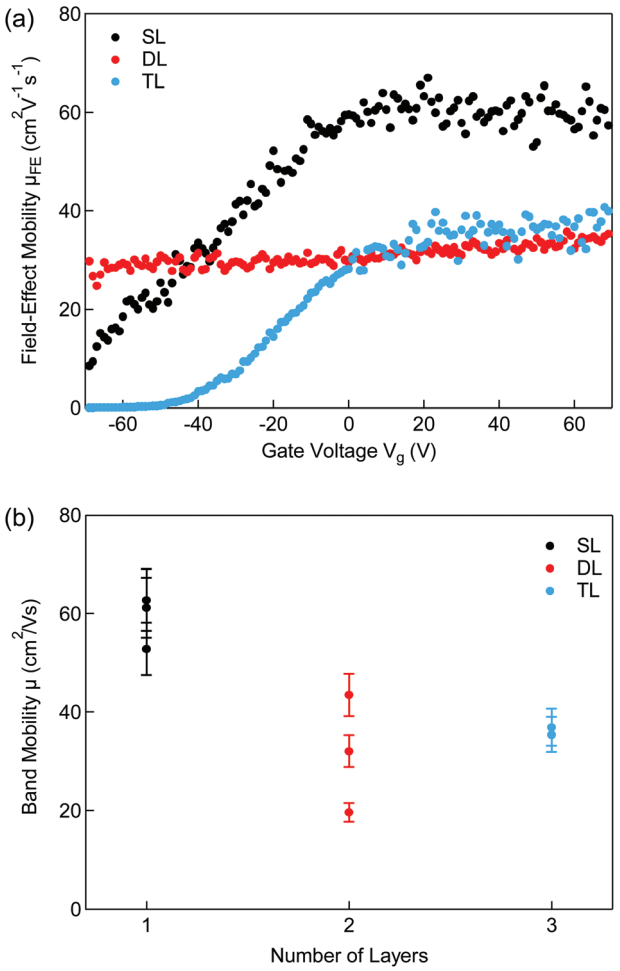

Fig. 3 Mobility in MoS_2 FETs after *in situ* annealing. (a) Mobility as a function of gate voltage V_g in selected mono-, bi-, and trilayer MoS_2 devices after *in situ* annealing at ~1×10^{-6} mbar. (b) Band mobility averaged over a range of ΔV_g = 10 V around the peak mobility as a function of number of layers for all characterized devices.

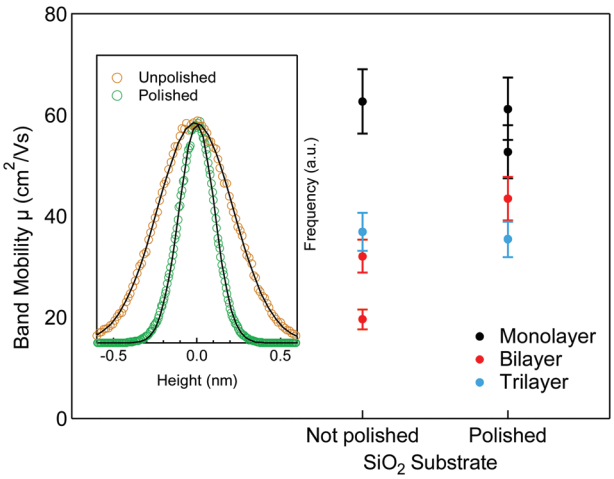

Fig. 4 Mobility in MoS_2 FETs on polished substrates. Band mobility as depicted in (b) sorted according to surface preparation. Inset: Histogram of the height distribution of unpolished and polished SiO_2 over an area of 2 μm × 2 μm measured with AFM. The black lines represent Gaussian fits.

mobilities have been reported. Nevertheless, this scattering mechanism cannot explain our experimental observation as it implies the opposite trend. Nor can scattering caused by intrinsic charged impurities explain the thickness-dependent mobility because such defects would equally affect all layer thicknesses. We thus attribute the higher mobility in a monolayer to a reduced effective electron mass relative to thicker layers.[27] It is interesting to note that the mobility trend is similar to the case of graphene.[28,29] We speculate that this similarity could arise from a reduction of phonon scattering modes in monolayers compared to thicker layers, enhancing the effect of lower effective mass in monolayer MoS_2.

We also investigate the correlation between surface roughness and mobility. In the case of graphene, it has been shown that devices exhibit improved performance if transferred onto boron nitride, which is attributed to the reduced surface roughness of this substrate.[30] Fig. 4 depicts the mobilities sorted for unpolished and polished SiO_2. As shown in the inset, the polishing of SiO_2 results in an ultra-smooth substrate. By this polishing, the RMS value of the surface height can be reduced from a value of ~250 pm to less than 150 pm (see Fig. SI 5 of ESI†). However, in the case of MoS_2, we do not detect a similar correlation between device performance and surface roughness.

We now compare the dynamics of performance degradation upon re-exposing the devices to ambient conditions (see Fig. 5). After *in situ* annealing, the vacuum is broken and the flakes are exposed to ambient air while their conductivity is monitored at a given value of V_{ds} = 100 mV and V_g = 70 V (Fig. 5a). The high gate voltage assures that the conductivity is modified by gaseous adsorbates in the range of band-like transport. To be able to compare the sensitivity for different devices, the conductivity $\sigma(t)$ is normalized, *i.e.* divided by $\sigma_0 = \sigma(t = 0)$. As can be seen in Fig. 5a, the monolayer is much more sensitive to exposure to atmosphere than the devices made of bilayer or trilayer MoS_2. It is reasonable to expect that the performance degradation upon exposure to ambient conditions is due to the adsorption of water and oxygen, with the dynamics governed by two characteristic time constants, with the shorter corresponding to the physisorption of oxygen (τ_1) and the longer to water condensation (τ_2). Because of this, we fit the experimental data with a double exponential of the form $\sigma/\sigma_0 = \sigma_0^n + \sigma_1^n \exp[-(t - t_0)/\tau_1] + \sigma_2^n \exp[-(t - t_0)\tau_2]$ and find a good agreement with the fit that can be explained by the presence of at least two different doping mechanisms. Fig. 5b shows the extracted time constants τ_1 and τ_2 for all layer thicknesses. τ_1 does not correlate with the number of layers and is of the order of 0.5–1.2 minutes. The τ_2 value of the monolayer (7.5 min.) is significantly smaller than for the bi- and trilayer (9.7–12.6 min.). In practice, many more gaseous species are physisorbed at the MoS_2 surface,[31] and a fit with multiple exponentials results in an even better fitting of the experimental data.

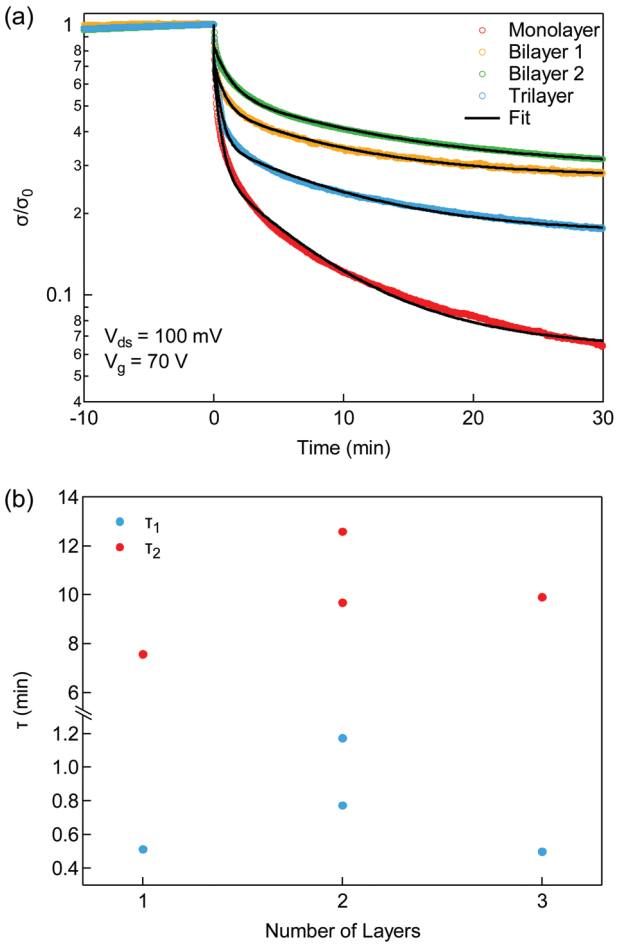

Fig. 5 Varying sensitivity of layers to atmosphere. (a) Normalized conductivity σ/σ_0, with $\sigma_0 = \sigma(t = 0)$, of one mono- two bi- and one trilayer MoS_2 device. The black line represents the double exponential fit described in the text. (b) Values of τ_1 and τ_1 extracted from the double exponential fit shown in (a).

Conclusion

In summary, we have compared the field-effect mobilities of FETs based on mono-, bi- and trilayer MoS_2 in vacuum after *in situ* annealing. We showed that the values attained on the mobility plateau are systematically higher in monolayer MoS_2 compared to bi- and trilayers. This contradicts previous results in which the effects of atmospheric adsorbates have not been removed. This in turn shows that it is crucial to take the influence of adsorbates and substrate properties into account. We demonstrate the importance of degassing adsorbates when trying to access the intrinsic properties of MoS_2, because monolayer MoS_2 is most sensitive to air exposure. This explains why it was so far believed to have a lower mobility. After reducing the influence of atmospheric contaminations, we can study the influence of surface roughness and show that it does not influence the mobility. Future experimental work should elaborate the precise adsorption processes of different gaseous species contained by ambient air, *e.g.* by means of FTIR, XPS or Auger spectroscopy. An important question that should be addressed by theoretical modeling is where the gaseous species are physisorbed exactly, *i.e.* is adsorption more likely to occur at defects and edges of the flake.

Acknowledgements

The authors gratefully acknowledge Z. Benes (CMi) for technical support with e-beam lithography and D. Bouvet (CMi) for support with chemical-mechanical planarization. This work was financially supported by ERC grant no. 240076 and carried out in the framework of the Marie Curie ITN network "MoWSeS" (grant no. 317451).

Notes and references

1 B. Radisavljevic, A. Radenovic, J. Brivio, V. Giacometti and A. Kis, *Nat. Nanotechnol.*, 2011, **6**, 147–150.
2 Q. H. Wang, K. Kalantar-Zadeh, A. Kis, J. N. Coleman and M. S. Strano, *Nat. Nanotechnol.*, 2012, **7**, 699–712.
3 K. S. Novoselov, A. K. Geim, S. V. Morozov, D. Jiang, Y. Zhang, S. V. Dubonos, I. V. Grigorieva and A. A. Firsov, *Science*, 2004, **306**, 666–669.
4 Y. Yoon, K. Ganapathi and S. Salahuddin, *Nano Lett.*, 2011, **11**, 3768–3773.
5 K. F. Mak, C. Lee, J. Hone, J. Shan and T. F. Heinz, *Phys. Rev. Lett.*, 2010, **105**, 136805.
6 B. Radisavljevic, M. B. Whitwick and A. Kis, *Appl. Phys. Lett.*, 2012, **101**, 043103.
7 B. Radisavljevic, M. B. Whitwick and A. Kis, *ACS Nano*, 2011, **5**, 9934–9938.
8 H. Wang, L. Yu, Y.-H. Lee, Y. Shi, A. Hsu, M. L. Chin, L.-J. Li, M. Dubey, J. Kong and T. Palacios, *Nano Lett.*, 2012, **12**, 4674–4680.
9 D. Krasnozhon, D. Lembke, C. Nyffeler, Y. Leblebici and A. Kis, *Nano Lett.*, 2014, **14**, 5905–5911.
10 D. Lembke and A. Kis, *ACS Nano*, 2012, **6**, 10070–10075.
11 O. Lopez-Sanchez, D. Lembke, M. Kayci, A. Radenovic and A. Kis, *Nat. Nanotechnol.*, 2013, **8**, 497–501.
12 S. Bertolazzi, J. Brivio and A. Kis, *ACS Nano*, 2011, **5**, 9703–9709.
13 S.-L. Li, K. Wakabayashi, Y. Xu, S. Nakaharai, K. Komatsu, W.-W. Li, Y.-F. Lin, A. Aparecido-Ferreira and K. Tsukagoshi, *Nano Lett.*, 2013, **13**, 3546–3552.
14 J. Kang, W. Liu and K. Banerjee, *Appl. Phys. Lett.*, 2014, **104**, 093106.
15 W. Bao, X. Cai, D. Kim, K. Sridhara and M. S. Fuhrer, *Appl. Phys. Lett.*, 2013, **102**, 042104.
16 D. Jariwala, V. K. Sangwan, D. J. Late, J. E. Johns, V. P. Dravid, T. J. Marks, L. J. Lauhon and M. C. Hersam, *Appl. Phys. Lett.*, 2013, **102**, 173107.
17 B. W. H. Baugher, H. O. H. Churchill, Y. Yang and P. Jarillo-Herrero, *Nano Lett.*, 2013, **13**, 4212–4216.

18 H. Schmidt, S. Wang, L. Chu, M. Toh, R. Kumar, W. Zhao, A. H. Castro Neto, J. Martin, S. Adam, B. Özyilmaz and G. Eda, *Nano Lett.*, 2014, **14**, 1909–1913.
19 H. Qiu, L. Pan, Z. Yao, J. Li, Y. Shi and X. Wang, *Appl. Phys. Lett.*, 2012, **100**, 123104.
20 P. Miró, M. Ghorbani-Asl and T. Heine, *Adv. Mater.*, 2013, **25**, 5473–5474.
21 M. M. Benameur, B. Radisavljevic, J.-S. Heron, S. Sahoo, H. Berger and A. Kis, *Nanotechnology*, 2011, **22**, 125706.
22 M. S. Fuhrer and J. Hone, *Nat. Nanotechnol.*, 2013, **8**, 146–147.
23 B. Radisavljevic and A. Kis, *Nat. Nanotechnol.*, 2013, **8**, 147–148.
24 B. Radisavljevic and A. Kis, *Nat. Mater.*, 2013, **12**, 815–820.
25 S. Das, H.-Y. Chen, A. V. Penumatcha and J. Appenzeller, *Nano Lett.*, 2012, **13**, 100–105.
26 R. Yang, Z. Wang and P. X. L. Feng, *Nanoscale*, 2014, **6**, 12383–12390.
27 W. S. Yun, S. W. Han, S. C. Hong, I. G. Kim and J. D. Lee, *Phys. Rev. B: Condens. Matter*, 2012, **85**, 033305.
28 N. Kosuke, N. Tomonori, K. Koji and T. Akira, *Appl. Phys. Express*, 2009, **2**, 025003.
29 S. V. Morozov, K. S. Novoselov, M. I. Katsnelson, F. Schedin, D. C. Elias, J. A. Jaszczak and A. K. Geim, *Phys. Rev. Lett.*, 2008, **100**, 016602.
30 C. R. Dean, A. F. Young, I. Meric, C. Lee, L. Wang, S. Sorgenfrei, K. Watanabe, T. Taniguchi, P. Kim, K. L. Shepard and J. Hone, *Nat. Nanotechnol.*, 2010, **5**, 722–726.
31 Q. Yue, Z. Shao, S. Chang and J. Li, *Nanoscale Res. Lett.*, 2013, **8**, 1–7.

